Effect of Pressure and Temperature on Colloidal Structure of Furrial Crude Oil

ARTICLE *in* ENERGY & FUELS · MARCH 2001

Impact Factor: 2.79 · DOI: 10.1021/ef000251t

2 AUTHORS:

Eric Y Sheu
University of Granada
82 PUBLICATIONS **2,069** CITATIONS
SEE PROFILE

Socrates Acevedo
Central University of Venezuela
111 PUBLICATIONS **1,270** CITATIONS
SEE PROFILE

Effect of Pressure and Temperature on Colloidal Structure of Furrial Crude Oil

Eric Y. Sheu*,† and Socrates Acevedo‡

Vanton Research Laboratory, Inc., 7 Olde Creek Place, Lafayette, California 94549, and Department of Chemistry, Central University of Venezuela, Caracas, Venezuela

Received October 30, 2000. Revised Manuscript Received January 18, 2001

The small-angle X-ray scattering technique was employed to investigate the colloidal structure of Furrial crude and its evolution as a function of pressure and temperature. A pressure cell with diamond windows and in situ pressure control was used to perform the pressure study between 1000 and 6000 psi. The temperature effect was examined between ambient and 150 °C. While the scattering spectra do not profoundly indicate appreciable change upon increasing pressure, the integrated scattering intensity over the scattering vector does indicate a systematic trend of structural dissolution with pressure. A polydisperse spherical structural model was applied to analyze the scattering data. The results revealed a systematic decreasing aggregate size with increasing pressure while the polydispersity of the aggregates increases drastically. On the other hand, both size and polydispersity decrease when temperature increases (up to 150 °C).

I. Introduction

Heavy oil is expected to dominate the fuel supply soon. This drives industrial research on how to efficiently produce and refine heavy oils. The oil production rate is normally controlled by the flow of the crude oil in the production pipe, which almost solely depends on the flowability of the crude oil. It is also known that the flowability of the crude oil depends on the pressure in the production pipe. To optimize the operational cost while maximizing the production rate, an optimized pressure in the down hole to control the flowability is essential. However, there is always a danger that the pressure may be too low to maintain a flowable crude oil, and result in precipitation of the heavy components in the crude oil. In a serious case, the precipitation may end up plugging the pipe, wellbore, and even the formation. This is an important subject. In the past few years, rich research literature and reports have been produced.[1-15]

A commonly accepted wisdom in oil production is that the precipitation occurs when pressure is lower than a critical point, and that the precipitation kinetics is rather nearly instantaneous.[11,16-17] Conventionally, a simply-minded engineering measure to prevent precipitation from happening is to maintain the pressure above a so-called bubble point, where a gaslike bubbling phenomenon is observed. Bubble point is thus widely used as the critical point for precipitation, as well as an operational warning sign. However, there are many issues associated with heavy oil production and its relevance with the down hole pressure and temperature. Therefore, a good strategy is needed to ensure efficient operation.[18]

Recently, some research reports pointed out that precipitation of crude oils on a colloidal scale may have started when the pressure is much higher than the bubble point and may continue even when the pressure is much below the bubble point. The precipitation kinetics appears to accelerate upon decreasing pressure.[17] This is to say that one may be able to use an earlier warning sign to avoid a fatal disaster. Moreover,

* Author to whom correspondence should be addressed.
† Vanton Research Laboratory, Inc.
‡ Central University of Venezuela.

(1) Pan, Huanquan; Firoozabadi, Abbas. Reservoir Engineering Research Inst., USA. *SPE Prod. Facil.* **2000**, *15* (1), 58–65.
(2) Wu, Jianzhong; Prausnitz, John M.; Firoozabadi, Abbas. *AIChE J.* **2000**, *46* (1), 197–209.
(3) Hammami, A.; Phelps, C. H.; Monger-McClure, T.; Little, T. M. *Energy Fuels* **2000**, *14* (1), 14–18.
(4) Victorov, Alexey I.; Smirnova, Natalia A. *Fluid Phase Equilib.* **1999**, 158–160, 471–480.
(5) Yang, Z.; Ma, C. F.; Lin, X.-S.; Yang, J.-T.; Guo, T.-M. *Fluid Phase Equilib.* **1999**, *157* (1), 143–158.
(6) Andersen, Simon Ivar; Lindeloff, Niels; Stenby, Erling H. *Pet. Sci. Technol.* **1998**, *16* (3 & 4), 323–334.
(7) MacMillan, D. J.; Tackett, J. E., Jr.; Jessee, M. A.; Monger-McClure, T. G. Marathon Oil Co., USA. *Proc.—Int. Symp. Oilfield Chem.* **1995**, 471–480.
(8) Victorov, Alexey I.; Firoozabadi, Abbas. *AIChE J.* **1996**, *42* (6), 1753–1764. Fotland, P. Norsk Hydro Res. Cent., Bergen, Norway. *Fuel Sci. Technol. Int.* **1996**, *14* (1 & 2), 313–325.
(9) Fotland, P. Norsk Hydro Res. Cent., Bergen, Norway. *Fuel Sci. Technol. Int.* **1996**, *14* (1 & 2), 313–325.
(10) Rivas, Orlando R.; Imteuep, S. A. *Venez. Vision Technol.* **1995**, *2* (2), 4–17.
(11) de Boer, R. B.; Leerlooyer, Klaas; Eigner, M. R. P.; van Bergen, A. R. D. *Koninklijke, SPE Prod. Facil.* **1995**, *10* (1), 55–61.
(12) Kokal, Sunil L.; Najman, Joseph; Sayegh, Selim G.; George, Albert E. *J. Can. Pet. Technol.* **1992**, *31* (4), 24–30.
(13) Burke, Nancy E.; Hobbs, Ronald E.; Kashou, Samir F. *J. Pet. Technol.* **1990**, *42* (11), 1440–1446.
(14) Wu, Jianzhong; Prausnitz, John M.; Firoozabadi, Abbas. *AIChE J.* **2000**, *46* (1), 197–209.
(15) Hammami, A.; Phelps, C. H.; Monger-McClure, T.; Little, T. M. *Energy Fuels* **2000**, *14* (1), 14–18.
(16) Szewczyk, V.; Thomas, M.; Behar, E. *Rev. Inst. Fr. Pet.* **1998**, *53* (1), 51–58.
(17) Jiang, J. C.; Patil, S. L.; Kamath, V. A. *Pet. Dev. Lab., Prepr.—Am. Chem. Soc., Div. Pet. Chem.* **1990**, *35* (3), 522–530.
(18) Speight, James G. *J. Pet. Sci. Eng.* **1999**, *22* (1–3), 3–15.

10.1021/ef000251t CCC: $20.00
Published on Web 00/00/0000 PAGE EST: 5.9

15(3), 702-707, 2001

one may be able to chemically or physically treat the crude oil more effectively at such pressure than close to the bubble point.

On the refining side, a similar situation occurs. Heavy components comprise the majority of the vacuum resids,[19] and the hydrogenation operation is pressure sensitive,[19-21] again, due to potential precipitation of the heavy components, such as asphaltene. A successful control of the pressure can benefit the yield, the catalyst life, and the hydrogenation efficiency. In this regard, accurate characterization of the precipitation phenomenon, as a function of the measurable parameters is a key step toward developing technologies for operation optimization.

Petroleum researchers have been always searching for new technology to lower the critical precipitation pressure in order to increase the production rate. The prerequisite for developing such a technology is to accurately characterize the precipitation kinetics and the structural evolution of the aggregates on the colloidal scale as a function of pressure and temperature. It was this intention that led us to initiate this work.

A number of high-pressure research reports[22-24] use live oils and laser turbidity to evaluate the critical pressure. However, public-domain papers on structural study and evaluation of the crude oil on the colloidal scale under pressure are very few. In 1992, Carnihan et al.[25] first designed a pressure cell suitable for use in an X-ray scattering experiment. These authors used this cell and synchrotron sourced X-ray (at the Brookhaven National Laboratory) to study the effect of pressure on asphaltene structure in solvent (40% solvent. These authors were true pioneers in applying this technique for oil phase and structural determination. Unfortunately, there were no follow-up studies in this area, partly due to limited access of proper X-ray radiation source/spectrometer, and partly due to difficulty in interpreting the scattering data.

With advances of the analysis scheme for scattering data and X-ray spectrometer in the past few years,[26-30] it is worth revisiting this technique and promoting it as an industrial tool for field applications. We made this attempt by using a true crude oil system, the Furrial crude, without solvents. This is the first structural study of a straight crude on the colloidal scale under high pressure. The Furrial crude oil was chosen as the model because it is a notorious crude, creating numerous production problems; and it has high asphaltene content (~7%).

The colloidal structures in the crude oil, if present, are likely due to asphaltene self-association. This phenomenon has been observed and described by many articles.[26-29] We employed a low-intensity (a rotating-anode-based X-ray source) small-angle X-ray scattering (SAXS) to investigate the colloidal structure because the synchrotron-based X-ray is often too strong for studying petroleum materials. It may destroy the light end components of the crude oil. In fact, this was a concern in 1993 when Carnihan et al. conducted the experiment.[25] Tremendous efforts were made by these authors to minimize this effect. The SAXS data were analyzed by using a polydisperse model, assuming the colloidal aggregates are spherical,[28,29] which was found plausible for asphaltenes from various sources.[28,29]

The scattering data obtained from this work do not indicate drastic change for pressure between 15 and 6000 psi. However, the integrated scattering intensity over the entire measurable scattering vector does suggest a systematic trend of structural dissolution with increasing pressure. The results extracted from the model analysis suggest that the average aggregate size decreases with increasing pressure while the polydispersity increases with the pressure. On the other hand, both size and polydispersity decrease when temperature increases (up to 150 °C).

II. Experimental Section

Furrial crude oil was used as received without further purification or modification. Before loading to the pressure cell, the crude oil sample was raised to 50 °C and sheared for approximately 30 min. The pressure cell used has a stainless steel body with one fixed diamond window while the other is movable and can be screwed in and out for easy sample handling. When the movable window is tightly mounted to the fixed one, the path length is 1.00 ± 0.01 mm.

The scattering volume is less than 0.25 mL while the total sample volume is about 2 mL to allow high-pressure compression. A pressure gauge of ±5 psi accuracy was used to interactively monitor the cell pressure. The pressure was driven and controlled by pumping CO_2 with a simple hand pump. To pump the pressure to 6000 psi, the CO_2 was cooled to near freezing point (~2 °C) before hand pumping.

Temperature was controlled by inserting two electric heating blocks into the stainless body of the cell and regulated by a temperature controller. The temperature was controlled between ambient and 150 °C.

The small-angle X-ray apparatus has a copper-target rotating anode operating at 4 kW using Kα line X-ray at 1.54 Å wavelength. The sample-to-detector distance was chosen to be 5 m. With this sample-to-detector distance and the diameter of the 2-D detector, the resulting Q (scattering vector) ranges from 0.01 to 0.3 $Å^{-1}$ which enable us to measure particle size from ~5 to 1000 Å.

III. Small-Angle X-ray Scattering Data

The SAXS scattering intensity represents the differential cross section per unit volume, $d\Sigma/d\Omega$, of the

(19) Carbognani, Lante; Espidel, Joussef; Carbognani, Natasha; Albujas, Leryn; Rosquete, Marisol; Parra, Liakarla; Mota, Jennifer; Espidel, Anita; Querales, Nancy. *Pet. Sci. Technol.* **2000**, *18* (5 & 6), 671–699.

(20) Yang, Ming-Gang; Eser, Semih. Fuel Science Program, Book of Abstracts, 216th ACS National Meeting, Boston, August 23–27, 1998.

(21) Chen, H. H.; Montgomery, D. S.; Strausz, O. P. *J. Res.* **1988**, *4* (1), 45–57.

(22) Ferworn, Kevin A.; Svrcek, William Y. *Structure and Dynamics of Asphaltenes*; Mullins, O. C., Sheu, Eric Y., Eds; Plenum: New York, 1998; pp 227–246.

(23) Ferworn, Kevin A.; Svrcek, William Y.; Mehrotra, Anil K. *Can. Ind. Eng. Chem. Res.* **1993**, *32* (5), 955–959.

(24) Srivastava, R. K.; Huang, S. S.; Dong, Mingzhe. *SPE Prod. Facil.* **1999**, *14* (4), 235–245.

(25) Carnahan, Norman F.; Quintero, Lirio; Pfund, David M.; Fulton, John L.; Smith, Richard D.; Capel, Malcolm; Leontaritis, Kosta. *Langmuir* **1993**, *9* (8), 2035–2044.

(26) *Asphaltene—Fundamentals and Applications*; Sheu, E. Y., Mullins, O., Eds.; Plenum Press: New York, 1995.

(27) Espinat, D. In *Structure and Dynamics of Asphaltene*; Mullins, O., Sheu, E. Y., Eds.; Plenum Press: New York, 1998.

(28) Sheu, E. Y.; Liang, K. S.; Sinha, S. K.; Overfield R. E. *J. Coll. Int. Sci.* **1992**, *153*, 399.

(29) Sheu, E. Y. Self-association of Asphaltene: Structural and Molecular Packing. In *Structure and Dynamics of Asphaltene*; Mullins, O, and Sheu, E. Y., Eds.; Plenum Press: New York, 1998.

(30) Eric, Y.; Sheu E. Y. *Phys. Rev. A* **1992**, *45*, 2428.

scattering material. For a noninteracting system with n_p number density of the scattering centers (particles),

$$\frac{d\sum}{d\Omega}(Q) = n_p P(Q) \quad (1)$$

$$Q = \frac{4\pi}{\lambda} \sin\frac{\theta}{2} \quad (2)$$

is the scattering vector, λ is the wavelength, and θ is the scattering angle. $P(Q)$ is the so-called form factor and is governed by the particle size and shape. When the scattering centers (or particles) are polydisperse, eq 1 becomes

$$\frac{d\sum}{d\Omega}(Q) = \frac{N}{V}\langle P(Q)\rangle \quad (3)$$

where $\langle P(Q)\rangle$ is an ensemble average of the size and shape of the particles in a unit volume of the system.

For certain particle shapes, $P(Q)$ has analytical expressions and can be easily computed. For example, $P(Q)$ for a spherical particle of radius R is

$$P(Q) = |F(Q)|^2, F(Q) = V(\bar{\rho} - \rho_s)\frac{3j_1(QR)}{QR} \quad (4)$$

where $\bar{\rho}$ is the average scattering length density of the particles, and $j_1(x)$ is the spherical Bessel function of the first kind. The scattering length density represents the scattering contrast between the media and the particles. In the case of Furrial crude oil, the media will be whatever nonstructured components and the particles will be whatever form measurable particles within the spatial resolution of the X-ray scattering Q range of the apparatus we used. The contrast in SAXS is the electron density difference between the particles and the media.

The process for analyzing a SAXS curve is to model the particles with a presumed particle shape and polydispersity and parametrize the scattering intensity expression with a set of adjustable parameters. Using this expression one can fit the experimental data to extract the values of these parameters.

Several scattering studies of asphaltenes colloids have reported that asphaltenes from various geological sources form more-or-less spherical aggregates in both organic solvents and crude oil environments. As for polydispersity, direct mass spectroscopy measurements of vacuum resid derived asphaltenes suggested a Schultz-like distribution function.[30-33] Although the distribution was for asphaltenes molecules, using this distribution function for aggregates is a natural extension. A review of how to unambiguously determine the shape of the particle using scattering data was discussed in details by Sheu.[29]

If one takes the particle shape as spherical and the Schultz distribution function as the polydispersity function, an analytical form of the scattering intensity function can be derived.[30]

(31) DeCanio, Stephen J.; Nero, Vincent P.; DeTar, Maureen M.; Storm, David A. *Fuel* **1990**, *69* (10), 1233–1236.
(32) Storm, David A.; DeCanio, Stephen J.; DeTar, Maureen M.; Nero, Vincent P. *Fuel* **1990**, *69* (6), 735–738.
(33) Sheu, Eric Y.; Storm, D. A. *Int. J. Mass Spectrom. Ion Processes* **1993**, *124* (3), 215–221.

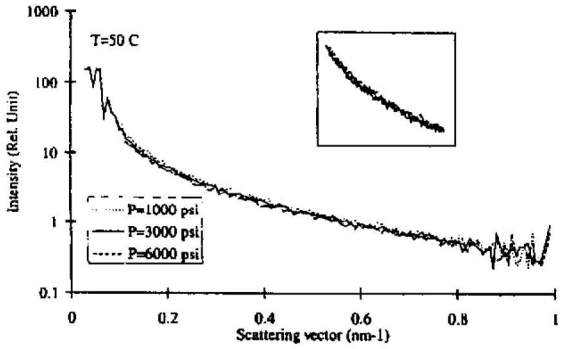

Figure 1. Scattering intensity as a function of pressures at $T = 50$ °C.

For a spherical particle with Schultz distribution the scattering intensity can be expressed as[30]

$$I(Q) = N_p(\Delta\rho)^2\langle P(Q)\rangle = N_p(\Delta\rho)^2\frac{\int G(Q,x)V_p^2(x)\,dx}{\int V_p^2(x)\,dx} \quad (5)$$

where N_p is the number density of the particles (aggregates), $\Delta\rho$ is the contrast (the electron density difference between media and the aggregates), V_p is the particle volume, $f(x)$ the particle size distribution function (the Schultz distribution function in this case with R = radius),

$$(R) = \frac{R^z}{\Gamma(z+1)}\left[\frac{(z+1)}{\bar{R}}\right]^{z+1}\exp^{-((z+1)R/\bar{R})} \quad (6)$$

where R is the average radius and $G(Q,R)$ is the form factor for a monodisperse sphere,

$$G(Q,R) = \left[\frac{3j_1(QR)}{QR}\right]^2 \quad (7)$$

Equations 5–7 were used to analyze the SAXS data using particle radius R and the polydispersity parameter z as the adjustable parameters. Once z is obtained, the polydispersity can be calculated according to

$$P(\%) = \frac{100}{\sqrt{z^2+1}} \quad (8)$$

The polydispersity index z in eq 6 is sensitive to the full width at half-maximum of the distribution function, thus provides good enough resolution for the polydispersity of the size distribution.

IV. Results and Analysis

Figure 1 shows the scattering intensity at 50 °C as a function of the pressure. One can more or less see that a trend of intensity decreases with increasing pressures. It is not as obvious but the trend appears to exist. The inset shows the Q range where the change of the intensity is most obvious. This may be considered as an indication of "dissolved" or "breakup" of the large structures into smaller structures at higher pressure.

However, the trend is not as obvious, likely due to the pressure range exercised, and is far from the critical

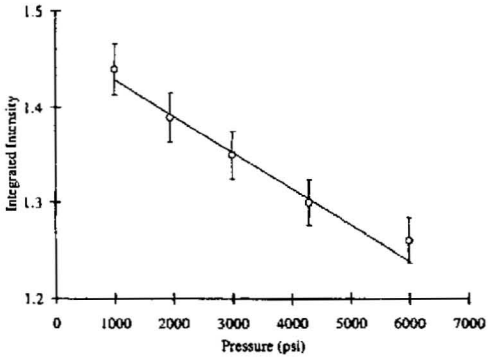

Figure 2. Integrated intensity for scattering vector = 0.015–0.6 nm^{-1} at 50 °C.

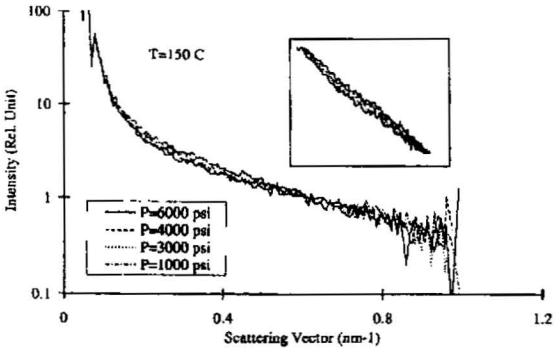

Figure 3. Same plot as Figure 1 for T = 150 °C

pressure where change is expected to be drastic.[23] Nevertheless, the effect is observable. The effect can be amplified by integrating the intensity along the Q axis. Figure 2 shows the integrated intensities at different pressures for Q from 0.15 to 0.06 $Å^{-1}$. This Q range was chosen because the corresponding particle size is about 20–200 Å which covers most of the aggregates that may create production problems, and $I(Q)$ shows that most changes occur at this range (see Figure 1). One should note that this integration was not used as intent to calculate the invariant, which provides the total surface area. If one attempts to calculate the invariant, a much lower Q range is needed to account for the larger particles. The integration performed here is to examine the change of the particles of size ranging from 20 to 200 Å.

As one can see from Figure 2, the intensity systematically decreases as pressure increases. The linearity may be a coincidence, but the decrease in intensity is real and should be regarded as the direct evidence that SAXS is sensitive enough to detect the subtle change of overall particle size distribution though the pressure is far from the critical point.

Figure 3 is the intensity plot for T = 150 °C. At this temperature, the decrease of $I(Q)$ is much more obvious than at 50 °C as shown in the inset. One can easily see decreasing intensity in the scattering vector range between ~0.2 to ~0.5 (nm^{-1}) for pressure from 1000 to 6000 psi. The integrated intensities from Q = 0.15 to 0.6 nm^{-1} is shown in Figure 4. Again, the intensity consistently decreases linearly. The phenomenon of the "dissolution" of the large structure appears to occur. It

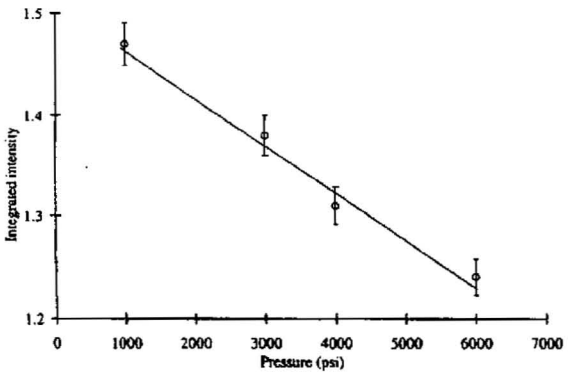

Figure 4. The same plot as Figure 2 for T = 150 °C.

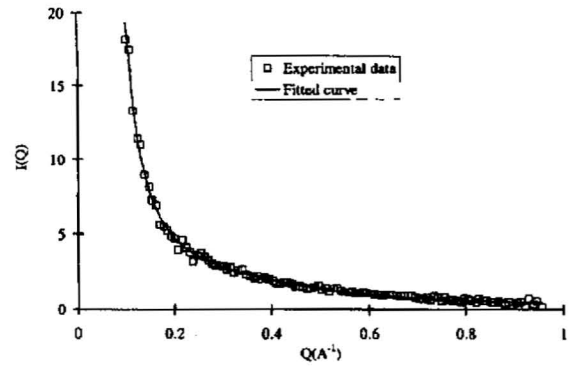

Figure 5. Analysis of Furrial crude oil at 150 °C, 3000 psi assuming particles are spherical with a Schultz size distribution.

is clear from both 50 and 150 °C results, one should redefine the long-standing wisdom that no precipitation occurs when the pressure is above the bubble point, and that when the bubble point is reached sudden precipitation occurs. The scattering data does not suggest such a zero-order transition. Rather, it indicates the process to be gradual on the colloidal scale.

An interesting point worth noting is the slope of the integrated intensity as a function of pressure. The slope of the integrated intensity at T = 150 °C is slightly higher than that at T = 50 °C. We interpreted this as an indication of faster loss of structure at higher temperature and higher pressure. It seems to make perfect sense but one should note that the integrated intensity at 150 °C is actually higher at lower pressure, which means that at 150 °C the system may have more structure than at 50 °C, if the pressure is low enough. In other words, the pressure dependence is more pronounced than the temperature dependence, at least in this case.

To evaluate the impact of pressure and temperature on particle size and distribution, a structural analysis is required. Previous experience with asphaltene scattering[28,29] suggested that the interparticle interactions are insignificant at the concentration level we are dealing with (<8 wt % asphaltene) and a polydisperse spherical model is accurate enough to characterize the structures of asphaltene aggregates.

Figure 5 shows a typical fitting analysis using a polydisperse spherical model. The agreement is excel-

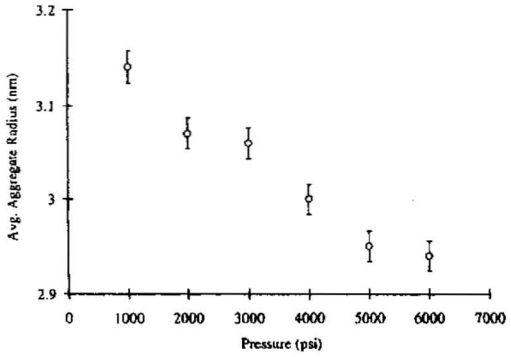

Figure 6. Structural evolution as a function of pressure at 50 °C.

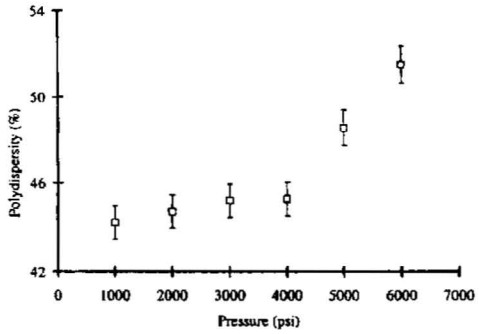

Figure 7. Polydispersity of the particles as a function of pressure at 50 °C.

Table 1. Extracted Parameters from SAXS Polydisperse Analyses

temperature (°C)	pressure (Psi)	avg. aggregate radius (nm)	polydispersity (%)
50	1000	3.14	44.19
50	2000	3.07	44.70
50	3000	3.06	45.19
50	4000	3.00	45.27
50	5000	2.95	48.56
50	6000	2.94	51.50
75	5000	2.93	45.56
100	5000	2.92	37.76
125	5000	2.89	33.90
150	5000	2.85	33.61
150	1000	2.99	30.52
150	2000	2.96	30.75
150	3000	2.91	31.70
150	4000	2.89	32.87
150	5000	2.85	33.61
150	6000	2.85	33.73

lent. The same model was applied to all the data collected and the agreement is similar to the case shown in Figure 5. The extracted structural and polydisperse parameters are tabulated in Table 1. The radii extracted are consistent with the results previously obtained from the Ratawi resid asphaltene particles in solvent[26] and those obtained by Espinat et al.[27]

Figures 6 and 7 show the average asphaltene aggregate radius and polydispersity as a function of pressure at 50 °C. The trends are clear. The radius decreases with increasing pressure while the polydispersity increases. The temperature effect at $p = 5000$ psi is illustrated in Figure 8 and Figure 9. The radius decreases with increasing temperature, which is expected. The polydispersity decreases drastically as temperature increases which is consistent with an earlier work by Sheu et al.[28] using toluene as solvent. Other than the trends observed, the decreasing and increasing functions do not seem to follow any particular functions.

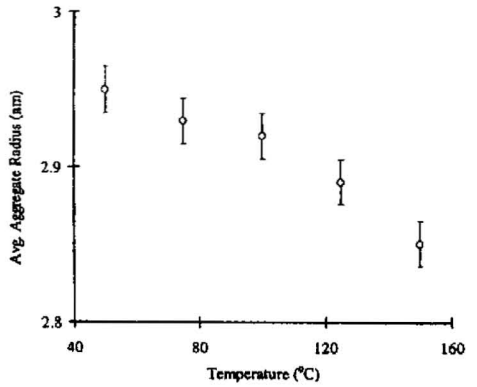

Figure 8. Average asphaltene aggregate radius as a function of temperature at $p = 5000$ psi.

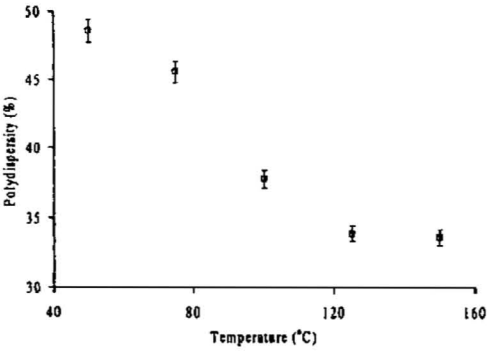

Figure 9. Polydispersity as a function of temperature at $p = 5000$ psi. A clear down trend is observed.

One also notes that the degree of variation upon pressure is in the neighborhood of 3 to 5% (compared to an error bar of 1.5−1.7%) which is considered minor, though can be picked by SAXS. The polydispersity is much more apparent, especially, as a function of temperature.

V. Discussion and Conclusion

The challenge in this experiment was that the absolute intensity was very hard to obtain because CO_2 was used as the compressing agent, which may dissolve in the crude oil and may associate with any components. This is to say that CO_2 may be found in both disperse and continuous phases with a partition coefficient, and the partition coefficient may vary with temperature and/or pressure. Thus, an accurate calculation of the contrast is difficult to obtain.

The reason CO_2 was chosen was because it is a common gas used to flood the formation. The problem of accurately account for the contrast is the reason one should be careful when interpreting the slope of the integrated intensity (see Figures 2 and 4). Our interpretation was that the intensity, when goes low as a function of pressure, means that the amount of the

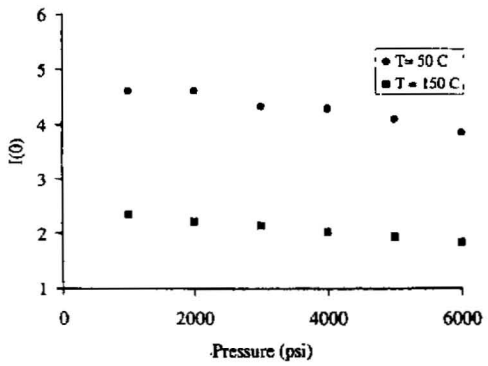

Figure 10. $I(0)$ as a function of pressure at $T = 50$ and 150 °C.

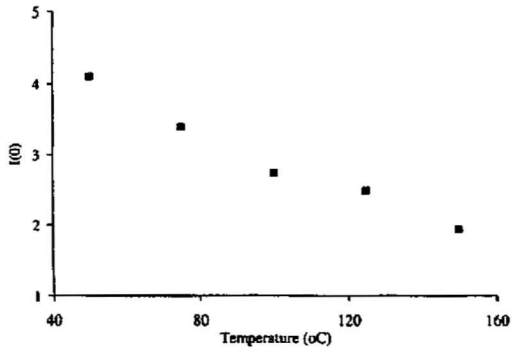

Figure 11. $I(0)$ as a function of temperature at $p = 5000$ psi.

particles within the selected size range decreases. This interpretation is not correct if the contrast changes at the same time. Therefore, we can only compare the slope of the intensity along the pressure axis for two temperatures and assume the contrast dependence on pressure follows a similar trend at these two temperatures. Even so, the interpretation may still be incorrect. Fortunately, there are two control point at 1000 and 6000 psi. At 1000 psi the intensity at 150 °C is higher than at 50 °C, while it is lower when $p = 6000$ psi. Combining these facts and the assumption of the contrast dependence, one can be more confident that particle size and distribution do change when T or P changes.

The similar difficulty happens when one tries to obtain the $I(0)$ which requires not only low Q data but also a reliable extrapolation scheme to $Q = 0$. Without low enough Q we can only use a simple minded linear extrapolation to obtain $I(0)$ which is considered approximate and will only be used for discussion rather than to present it as a result of this work. Figure 10 shows this plot (the error bars are small than the symbol sizes).

Because the absolute intensity cannot be obtained accurately, the contrasts cannot be accurately determined. As a result, only relative $I(0)$ of each scattering spectrum can be obtained. If one examines $I(0)$ obtained (see Figure 10), one again sees the trend of decreasing intensity upon increasing pressure. One may argue that the decreasing intensity is due to contrast change. If it is the case, the data show a decreasing contrast between solvent and the particles. Since the particles (likely formed by asphaltenes) have high packing energy as indicated in temperature study,[28,34] one would expect the particle packing remains rigid unless part of the structure breaks away. In this situation, only filling the CO_2 into the cavities of the rigidly formed structure can change the contrast and the change will be similar for 1000 and 6000 psi. If this is correct, the decreasing intensity can be attributed to the breaking away of the dispersed structural.

A similar $I(0)$ plot for evaluating the temperature effect is shown in Figure 11 (the error bars are smaller than the symbol sizes). The same trend follows, meaning that the aggregates "dissolve" upon increasing temperature as reported in the solvent case.[28] However, one note that the absolute intensities were not obtained experimentally; the trends shown here are qualitative and should only be used as a reference, instead of treating these data (Figures 10 and 11) as results.

In conclusion, this series of SAXS measurements demonstrate that subtle structural change occurs when pressure varies and it can happen even whenthe pressure is far from the bubble point. The other point made here is that SAXS is an appropriate technique to detect this subtle change.

The analyses show that the particle size change is minimal, though can be detected by SAXS. The polydispersity gives better quantitative indication. Due to such a small change (3–5%), one needs to use an appropriate structural model, to properly extracted the structural quantities.

Although the changes are detectable by SAXS, the underlying physics of how the structure evolves is still unknown. The intension of reporting these results is to lay a foundation of a potential technique for detecting the precipitation propensity of heavy oils during production. In addition, this technique may be applicable for evaluating the effect of the chemicals commonly used for well treatment.

Acknowledgment. The authors thank Dr. J. S. Lin of Oak Ridge National Laboratory for granting SAXS beam time for performing this experiment. This project was partially supported by the Venezuelan CONICIT Project (Project Number 97004022). We also acknowledge the work by Carnihan et al., which inspired us to perform this experiment.

EF000251T

(34) Overfield, R. E.; Sheu, E. Y.; Sinha, S. K.; Liang, K. S. *Fuel Sci. Technol. Int.* **1989**, *7* (5–6), 611.